OCS Study
MMS 2004-008

Low Frequency Waves in the Santa Barbara Channel Observed by High Frequency Radar

Final Technical Summary

Final Study Report

U.S. Department of the Interior
Minerals Management Service
Pacific OCS Region

OCS Study
MMS 2004-008

Low Frequency Waves in the Santa Barbara Channel Observed by High Frequency Radar

Final Technical Summary

Final Study Report

Authors
Edwin Beckenbach
Libe Washburn

Principal Investigators
Libe Washburn
Steven Gaines

Prepared under MMS Cooperative
Agreement No. 1435-01-00-CA-31063
by
Coastal Marine Institute
Marine Science Institute
University of California
Santa Barbara, CA 93106

U.S. Department of the Interior
Minerals Management Service
Pacific OCS Region

Camarillo
January 2004

Disclaimer

This report has been reviewed by the Pacific Outer Continental Shelf Region, Minerals Management Service, U.S. Department of the Interior and approved for publication. The opinions, findings, conclusions, or recommendations in this report are those of the authors, and do not necessarily reflect the views and policies of the Minerals Management Service. Mention of trade names or commercial products does not constitute an endorsement or recommendation for use. This report has not been edited for conformity with Minerals Management Service editorial standards.

Availability of Report

Extra copies of the report may be obtained from:

U.S. Dept. of the Interior
Minerals Management Service
Pacific OCS Region
770 Paseo Camarillo
Camarillo, CA 93010
Phone: 805-389-7621

A PDF file of this report is available at:
http://www.coastalresearchcenter.ucsb.edu/CMI/

Suggested Citation

The suggested citation for this report is:

Beckenbach, Edwin and Washburn, Libe. Low frequency waves in the Santa Barbara Channel observed by high frequency radar. MMS OCS Study 2004-008. Coastal Research Center, Marine Science Institute, University of California, Santa Barbara, California. MMS Cooperative Agreement Number 1435-01-00-CA-31063. 43 pages.

Table of Contents

List of Tables and Figures

Technical Summary

Final Study Report

FINAL TECHNICAL SUMMARY

STUDY TITLE: Observing the surface circulation along the South-Central California Coast using high frequency radar: consequences for larval and pollutant dispersal

REPORT TITLE: Low frequency waves in the Santa Barbara Channel observed by high frequency radar

CONTRACT NUMBER: 1435-01-00-CA-31063

SPONSORING OCS REGION: Pacific

APPLICABLE PLANNING AREA(S): Southern California

FISCAL YEAR(S) OF PROJECT FUNDING: FY 01, FY 02

COMPLETION DATE OF REPORT: December 2003

COSTS: FY 01 - $108,017; FY 02 - $115,983; FY 03 - no cost

CUMULATIVE PROJECT COST: $224,000

PROJECT MANAGERS: Russell J. Schmitt

AFFILIATION: University of California, Santa Barbara

ADDRESS: Coastal Research Center, Marine Science Insitute, University of California, Santa Barbara, CA 93106

PRINCIPAL INVESTIGATORS: Libe Washburn[1], and Steven Gaines[2]

ADDRESS: [1]Professor, Institute for Computational Earth System Science, Dept. of Geography, University of California, Santa Barbara, CA 93106-3060; [2]Professor, Dept. of Ecology, Evolution, and Marine Biology, Biology, California, Santa Barbara, CA 93106

KEY WORDS: Central and Southern California, coastal, Point Conception, Santa Barbara Channel, coastal circulation, high frequency radar, coastal trapped waves, topographic Rossby modes, rock fishes

BACKGROUND:

An array of high frequency radars along the South-Central California coast for oceanographic studies

High frequency (HF) radars are becoming more common in studies of ocean circulation around the coasts of the United States. It is anticipated that HF radars will be key components of evolving coastal ocean observing systems (e.g. oceans.us web site: http://www.ocean.us/) since they are the only technology now available which can produce time series maps of surface currents round the clock. Other technologies such as arrays of moorings are prohibitively expensive for this purpose, although mooring arrays complement HF radars by supply critical sub-surface velocity and water property data.

An array of HF radars has been operating in the Santa Barbara Channel since 1998 with observations being made from up to five sites. The current configuration of the array with three HF radar systems is shown in Fig. 1. Radar hardware was obtained through grants from the W.M. Keck Foundation and the University of California Marine Council. Two systems were borrowed from NOAA's Environment Technology laboratory in Boulder Colorado. Operational support for the radar array has come from a number of agencies: Minerals Management Service, Partnership for Interdisciplinary Studies of Coastal Oceans (PISCO), University of California Marine Council, and NASA.

Throughout most of this study, each radar system produced time series of radial current components (hereafter referred to as "radials") out to a maximum range of 40 km off shore. More recently, software advances in the systems have allowed radials to be obtained out to a maximum range of 60 km. As discussed by Emery et al. (2004), the actual range and overall coverage area of the radars varies over a wide range of time scales with a prominent diurnal component. For the 12-13 MHz systems used in this study, radials are obtained as spatial averages over sectors of the sea surface measuring 5 degrees in azimuth by 1.5 km in range. Radials in each sector are computed over 10 minute intervals. Total current velocity vectors are estimated by averaging all radials each hour observed over circular areas of the sea surface with 3 km radii. The circles are centered on points on a square grid with two km spacing between points. The least square technique described by Gurgel (1994) is used to combine radials within the circular areas to estimate the eastward and northward current components at each grid point. Figure 1 shows examples of surface current vectors computed on the 2 km grid on 23 June 2003 at 1200 GMT.

Figure 1. High frequency radar array in the Santa Barbara Channel as of December 2003. Diagram shows surface current vectors on 23 June 2003 at 1200 GMT. Radar systems are indicated by triangles at Refugio State Beach, Coal Oil Point, and the Mandalay Generating Plant near Oxnard California. Scale for surface current vectors is shown at left along with size of circles used in estimating surface current vectors. Box on map of California (upper right) shows study area. CES-SIO current meters SMIN, SMOF, and AMNI are indicated with circles. Current vectors are placed on a 2 km grid.

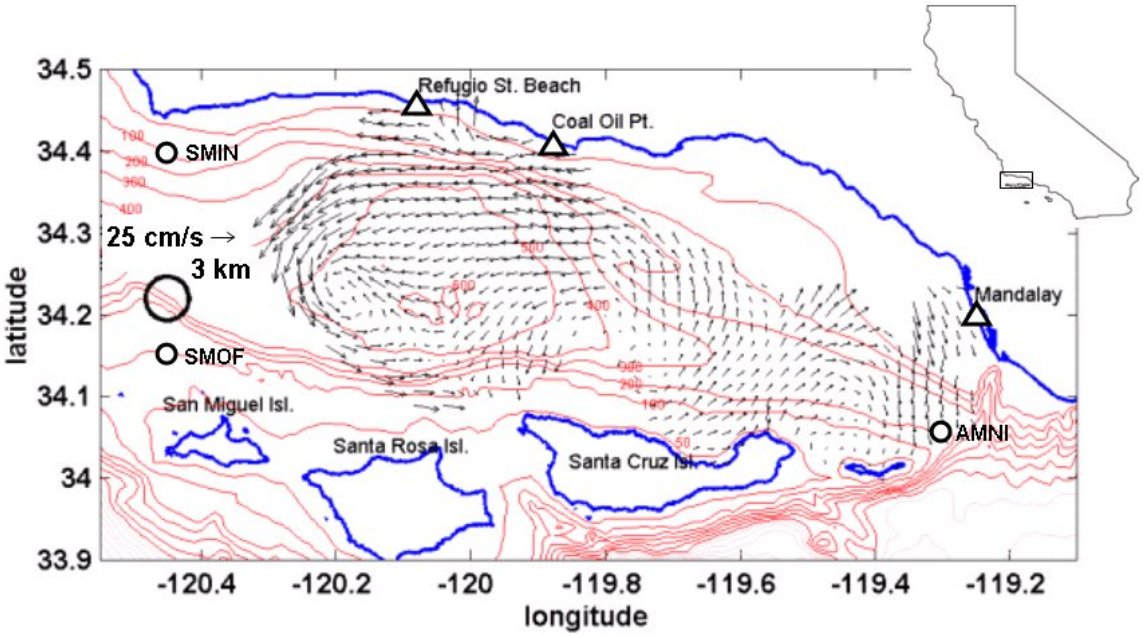

Emery et al. (2004) describe the performance of the array by comparing surface currents obtained from the HF radars with an extensive array of moored current meters. The current meters were deployed by the Center for Coastal Studies at the Scripps Institution of Oceanography (CES-SIO). Four of these current meters are still in operation and three of them are shown with circles in Fig. 1. Data from the current meters were kindly made available to this project by CES-SIO personnel. Emery et al. (2004) found that the HF radar-derived and current meter-derived radial time series were significantly coherent for time scales of about 11 hours and longer. Hourly radial measurements were significantly correlated for all radar-current meter pairs with r^2 ranging from 0.5 – 0.7. Results of this study focus on current variability on sub-tidal time scales (36 hours and longer) since correlation between the radars and current meters was greatest for these time scales.

OBJECTIVES:

Our research examined various aspects of the surface circulation in the western Santa Barbara Channel and Santa Maria Basin with a particular focus on the following questions related to physical oceanography:

1. What are the spatial and temporal scales of eddy variability?
2. How is local wind forcing related to the surface circulation?
3. How stable is the cyclonic circulation in the Santa Barbara Channel?

4. How does the offshore flow influence flow on the inner shelf?

The following questions related to marine ecology were also addressed in the research:

1. Are dominant spatial patterns of recruitment linked to transient surface circulation features or to the time-averaged, "mean" flow?
2. Is offshore flow at Pt. Conception important in maintaining the bio-geographic boundary there?
3. Do poleward flow events lead to recruitment north of Pt. Arguello?
4. Is local retention or remote supply more important in maintaining various marine populations on the south-central California coast.

An operational goal of this research was to provide near-real time observations of surface currents in support of scientific research, management decision making, and other operations such as search and rescue.

DESCRIPTION:

Low frequency waves in the Santa Barbara Channel

Previous observations in the western Santa Barbara Channel (SBC) have show that a dominant feature of the circulation there is a persistent cyclonic pattern of rotating currents (e.g. Harms and Winant (1998), Dever (2004). These and other observations showed that this cyclonic circulation is highly variable on time scales of a few days and longer. An important research focus of this study was an examination of propagating eddy-like features reported by Nishimoto and Washburn (2002) which disrupted the cyclonic circulation on time scales of about two weeks. Initial analysis suggested that these features were some type of eddy which formed to the east and then propagated into the radar coverage area. A three-year time series of HF radar observations of surface currents in the western Santa Barbara Channel (SBC) was used to examine these propagating features. This analysis, as summarized in the Study Report following this Technical Summary, indicates that the motions are not freely propagating eddies as we initially hypothesized, but are a type of large scale wave motion.

The features appear as sequences of alternating cyclonic (counter-clockwise) and anti-cyclonic (clockwise) vortices propagating westward with a period of about two weeks. The sequences often last up to a few months and occur intermittently throughout the year. No distinct seasonal trend was found. The surface velocity patterns of the cyclones, when reversed, are very similar to those of the anticyclones, which indicates a high degree of anti-symmetry. (Antisymmetry is used here to indicate that the velocity patterns of the cyclones and anticyclones are nearly "mirror-images" of each other.) Both the cyclones and anticyclones have mean propagation speeds of ~5 km day^{-1} and relative vorticity magnitudes of order 0.1 f, where f is the local Coriolis parameter (The Coriolis parameter is a measure of the strength of the Coriolis force at a given latitude. It is zero at the equator and increases toward the North Pole). The anti-symmetry of the features was remarkable as described in the Study Report. These propagating vortices resemble the propagating cyclones with periods of 10 - 25 days reported in the SBC by Harms and Winant (1998).

The dominant propagating patterns were extracted using an objective analysis technique described by Wallace (1972) called complex empirical orthogonal function (CEOF) decomposition. The method was applied to surface velocity data which had been band-pass filtered to eliminate variance outside the 10-20 day pass band. Coherence analysis of the HF radar data had revealed that the propagating features dominated the velocity variance in this band. The CEOF analysis separated the variance into two dominant modes. The first mode with an average period of 14.4 days explains 45% of the velocity variance and represents the alternating cyclones and anticyclones that are evident in the band-pass filtered record. The second mode, with an average period of 13.3 days, explains 25% of the velocity variance and mainly represents alongshore current fluctuations. Amplitude functions of the two modes correlate with *in situ* current time series at 5 and 45 m depths obtained from the CES-SIO moorings at the east and west channel entrances. This suggests coupling between the modes and the larger-scale circulation of the northern Southern California Bight.

These results are consistent with previous observations in the SBC. Auad and Henderschott (1997), Auad et al. (1999) investigated the relationship between low-frequency flow in the 6 to 18 day band and forcing by wind stress and remote adjusted sea level. The remotely-forced flow was explained as a coastal trapped, low-mode hybrid-wave with characteristics of both Rossby and Kelvin waves. The higher spatial resolution HF radar observations of this study support this interpretation since the period and along-shore flow of mode 2 are consistent with coastal trapped waves.

We hypothesize that mode 1 observed in this study is a resonant response of the Santa Barbara Basin in the form of a trapped topographic Rossby mode (TRM). A stream function representation of the mode 1 resembles the predicted pattern based on a simplified analytical model of a fundamental TRM in a closed basin. Peak relative vorticity over the basin is about a factor of four higher than over the edges, indicating topographic control by the basin. The amplitude of mode 1 is consistently large when the frequency difference between modes 1 and 2 is small. This suggests that the propagating vortices of mode 1 are a basin-scale resonant response to the coastal trapped wave represented by mode 2. A more complete discussion of this analysis is given in the Study Report and also by Beckenbach and Washburn (2002), Beckenbach and Washburn (2004).

Wind driven circulation in the Santa Barbara Channel

As discussed by Beckenbach (2004), the wind patterns over the SBC are well described by the first two modes of an empirical orthogonal function (EOF) decomposition. Together they explain 80-90% of the variance in the wind field for National Data Buoy Center (NDBC) buoys in and around the channel and are consistent with previous studies such as Dorman and Winant (2000).

Conditional averaging of the HF radar derived current fields for times when the modes 1 and 2 exceed ± 1 standard deviation reproduce the upwelling, relaxation, and convergent states such as described by Harms and Winant (1998), Dever (2004). The new information compared with previous studies is an improved description of circulation patterns in the interior of the SBC. The interior flow patterns agree with those inferred from surface drifters

(e.g. Dever et al., 1998). The flow patterns of the upwelling and convergent states are also consistent with the dynamical model of Oey et al. (2001): the upwelling flow state prevails when the along-channel wind stress gradient is small over the channel (even though the wind stress itself is large); cyclonic flow prevails when the wind stress gradient is large.

A principal advantage of HF radar for observing surface circulation patterns is its ability to produce two-dimensional current maps which allows computation of the important quantities of relative vorticity ζ and divergence. The average ζ pattern computed from a 4-year record shows the strong cyclonic flow, characteristic of the western SBC and consistent with previous studies showing cyclonic circulation (Fig. 2a). Mean values of ζ/f are as large as ~0.4 which means that secondary flow effects, such as localized upwelling or downwelling, are important (e.g. the so-called geostrophic balance does not strictly apply). Closely spaced streamlines in Fig. 2a (solid and dotted lines) indicate a strong westward current along the mainland coast which turns to the south on the western side of the Santa Barbara Basin.

Figure 2. a) Contours of mean relative vorticity ζ normalized by the Coriolis parameter f. Red shades indicate positive ζ/f and a counter-clockwise turning of velocity vectors. Blue shades indicate negative ζ/f and a clockwise turning of velocity vectors. Streamlines are indicated by lines, solid for positive, dotted for negative. These also correspond to lines of constant sea surface elevation with solid lines indicating elevated sea surface and dotted lines indicating lowered sea surface elevation. Means are computed from a 4-year record 1998-2001. **b)** Contours of the mean divergence of surface currents, div u. Blue shades are negative indicating convergence and downwelling; red shades are positive indicating divergence and upwelling. Contours of velocity potential are indicated by lines, solid for positive, dotted for negative.

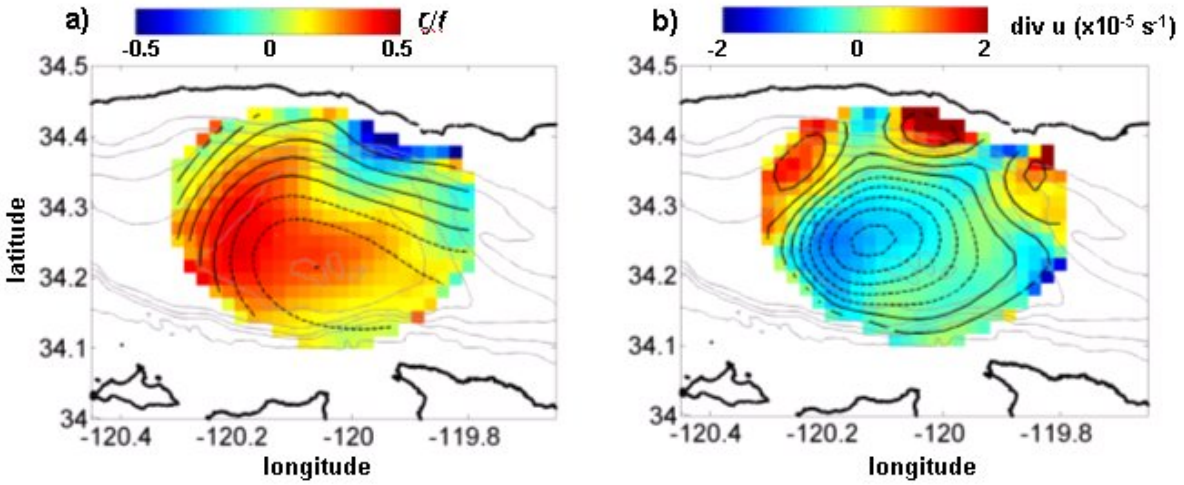

The pattern of divergence of horizontal velocity (div u) indicates a broad region of convergence consistent with downwelling in the channel interior (Fig. 2b). This is an unexpected result since the mean wind patterns generally favor upwelling and divergence. This pattern is currently being explored in collaboration with meteorologists Clive Dorman of SIO and Darko Koracin of the University of Nevada, Reno. An alternating pattern of positive and negative divergence on scales of ~10 km is prominent along the mainland coast. This pattern is consistent with a simple model of the advection of ζ as described in more detail by Beckenbach (2004). Lines in Fig. 2b show velocity potential contours which indicate the

strength of the divergent part of the surface current field. Solid and dotted lines indicate flow direction such that the local velocity vectors are perpendicular to them and point from high to low contour levels.

Circulation patterns around Point Conception

A combination of these HF radar observations and inner shelf moorings (funded by the Packard foundation as part of PISCO) are being used to explain circulation patterns around Pt. Conception. Knowing the circulation patterns around the point is important for understanding the movement of pollutants like oil and for describing the bio-geographic species range boundary found there.

Figure 3. a) Current vectors at mid-shelf locations conditionally averaged by flow state: red for the relaxation state, blue for the upwelling state, and green for the convergent state. Circles indicate moorings SAMI, SMIN, and AMNI deployed by CES-SIO (see Harms and Winant, 1998). HF1, HF2, and HF3 indicate surface current vectors from the HF radars at selected locations. **b)** Current vectors at inner shelf locations conditionally averaged by flow state as in panel a). Circles indicate moorings deployed at 10-15 m depths as part of the Partnership for Interdisciplinary Studies of Coastal Oceans (PISCO). Square shows location of NDBC buoy 46023.

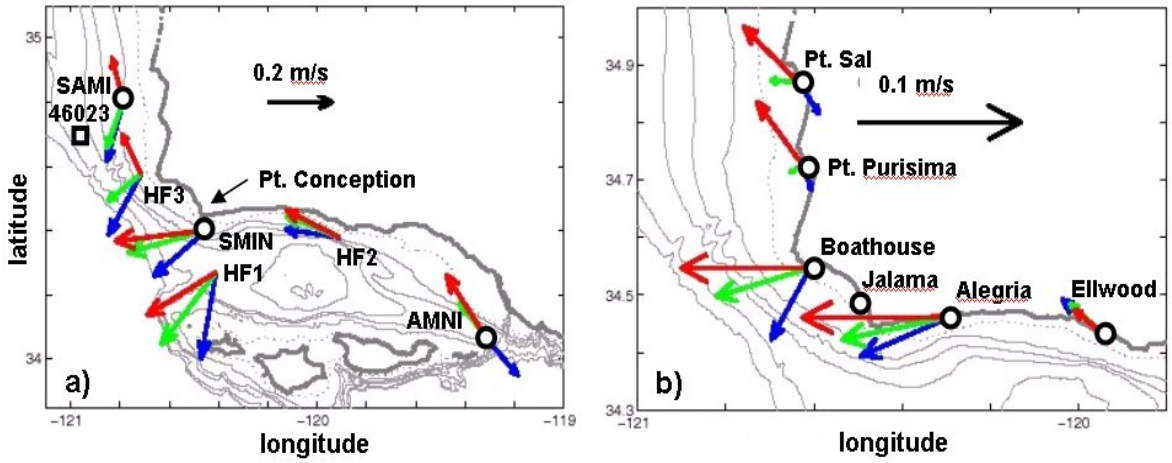

Cudaback et al. (2004) find that flow patterns on the inner shelf (10-15 m water depths) generally mimic those over the mid-shelf when conditionally averaged by the flow states of relaxation, upwelling, and convergence using the classification scheme of Dever (2004). However, flow speeds over the inner shelf are usually smaller by factors of three to five. Figure 3a shows current vectors conditionally averaged by flow state at points over the mid-shelf (100 m water depth for SMIN and SAMI; 200 m for AMNI). Data were obtained at the CES-SIO moorings of SAMI, AMNI, and SMIN (naming scheme described by Harms and Winant, 1998) and at HF radar grid points labeled HF1, HF2, and HF3. Vectors are color coded as: red for relaxation, blue for upwelling, and green for convergence. Overall, conditionally averaged current vectors over the inner shelf (Fig. 3b) are generally similar to those over the mid-shelf.

North of Pt. Conception the relaxation state produces poleward flow at all locations over the mid and inner shelf. At SMIN, HF1, HF2 and AMNI, the relaxation state forces generally westward flow. In contrast, the upwelling state produces flow with strong equatorward

components over the mid and inner shelf, except for HF2 and Ellwood which are poleward. At Boathouse the upwelling state produces strong equatorward flow consistent with the upwelling center found at Pt. Conception. The convergent state produces larger differences in current direction between the mid and inner shelf north of Pt. Conception. At mid-shelf locations SAMI and HF3 the convergent state produces equatorward flow while on the inner shelf at Pt. Sal and Pt. Purisima, the flow is mostly offshore. In the channel, flow on the mid and inner shelf is poleward for the convergent state.

Other important differences between mid and inner shelf also exist. One of the greatest differences is that for many wind relaxation events, warm waters flow poleward over the inner shelf while equatorward flow prevails over the mid-shelf. This means that relaxation events over the inner shelf are often not accurately predicted using mid-shelf circulation patterns.

Figure 4. a) Wind speed at NDBC buoy 46023. **b)** Time series of principal axis current speed at inner shelf mooring Pt. Purisima (green) and mid-shelf mooring SAMI (black) for June – October, 2000. Positive currents are poleward. Vertical dashed lines indicate three relaxation events of weak or poleward winds. Poleward flow occurs at Pt. Purisima for wind relaxation events 1 and 2, but not at SAMI. Poleward flow occurs at both Pt. Purisima and SAMI for Event 3. **c)** Position-time contours of sea surface temperature for inner shelf moorings Ellwood, Alegria, Jalama, Boathouse, Pt. Purisima, and Pt. Sal. Locations of moorings and NDBC buoy 46023 are shown in Fig. 3a. Arrow shows poleward propagation of warm water around Pt. Conception at ~13 km day^{-1} in June 2000.

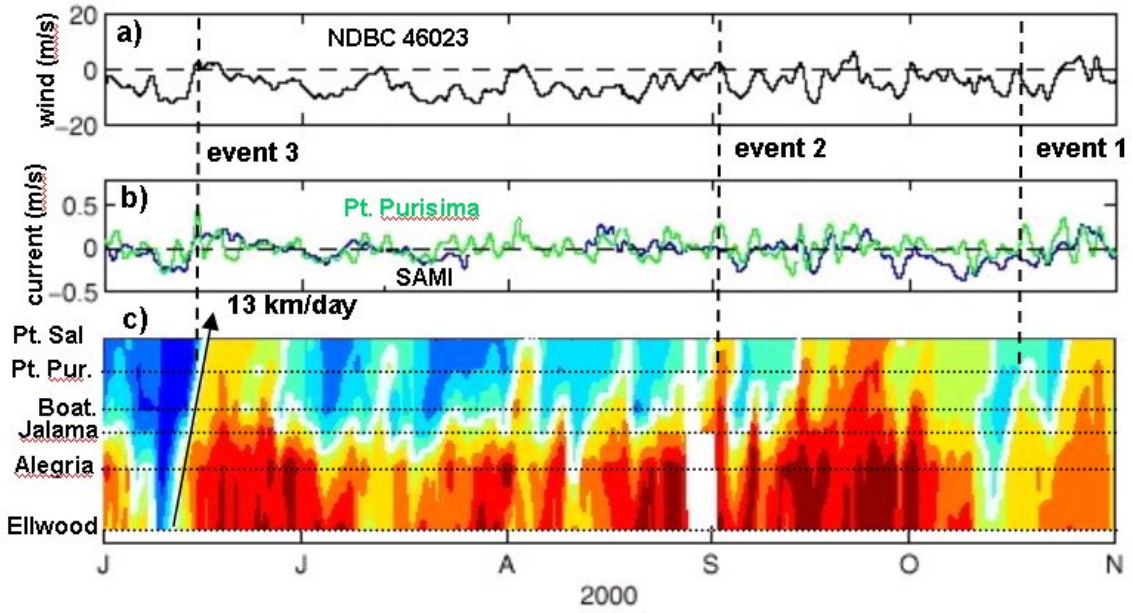

An example of the response of the inner shelf to wind relaxation is shown in Figure 4 as event 1 when winds were almost zero (Fig. 4a). At this time currents flowed poleward at Pt. Purisima, but equatorward at SAMI (Fig. 4b). This event was accompanied by warm water reaching Pt. Purisima (Fig. 4c). A similar situation occurs during event 2, but in this case the winds reversed producing poleward flow at Pt. Purisima and nearly zero flow at SAMI. During event 3 flow was poleward at both Pt. Purisima and SAMI as warm water advected northward at ~13 km day^{-1} (arrow, Fig. 4c).

Cudaback et al. (2004) find that poleward flow over the inner shelf is quite common year round as suggested by Fig. 4. This indicates that northward flow pathways for pollutants and larvae are fairly common year round. Furthermore, it suggests that the bio-geographic boundary at Pt. Conception is not simply due to flow since flow pathways around the point are frequent. We are currently exploring the effects that these warm flow events might have on organisms in inter-tidal habitats north of Pt. Conception.

SIGNIFICANT CONCLUSIONS:

Surface circulation

This study supports the following conclusions about the surface circulation in the western Santa Barbara Channel:

1. Variability in the persistent cyclonic eddy-like circulation is controlled by a combination of local wind forcing and remote forcing by coastal trapped waves. An important conclusion of this study is that topographic Rossby modes exist in the channel over the Santa Barbara Basin and dominate the circulation in the 10-20 day band.
2. Topographic Rossby modes appear as sequences of propagating eddy-like features with horizontal scales of about 30 km. The sequences last up to a few months and occur intermittently throughout the year. The surface velocity distribution of cyclones and anticyclones are anti-symmetric with a mean propagation speed of ~5 km day^{-1} and relative vorticity magnitudes of order 0.1 f, where f is the local Coriolis parameter.
3. The topographic Rossby modes appear to be forced by propagating coastal trapped waves which have been described in previous studies (e.g. Auad and Henderschott (1997), Auad et al. (1998)
4. Conditional averaging based on the wind field shows that two-dimensional surface flow patterns over the inner shelf (10-15 m water depths) are strongly coupled to the wind field in the western Channel. Strong along-channel wind gradients coincide with cyclonic circulation and the so-called convergent flow state (e.g. Dever, 2004). Weak along channel wind gradients coincide with broad equatorward flow on the inner shelf and the upwelling state. Weakening or reversals of the wind patterns coincide with strong cyclonic circulation and strong poleward flow along the inner shelf of the mainland coast.
5. Flow over the mid-shelf as observed by HF radar and an array of moorings shows that inner shelf flow patterns (10 - 15 m water depths) is often qualitatively similar to flow patterns over the mid-shelf (100 m water depths) for the upwelling state and, to a lesser extent, for the convergent state.
6. Flow over the inner shelf appears to respond more strongly to relaxation events and reversals in the wind field than does the mid-shelf. Events frequently occur in which poleward advection of warm waters frequently occurs on the inner shelf, but not on the mid-shelf.

Marine Ecology

This study supports the following conclusions related marine ecology and pollution transport: the research:

1. The predominant circulation pattern in the vicinity of Point Conception, CA probably cannot account for the bio-geographic boundary there because of the frequent occurrence of flow reversals on the inner shelf associated with wind relaxation events.
2. Northward transport around Point Conception, CA of pollutants and larvae of marine organisms, is more likely near shore during wind relaxation events than in deeper waters offshore. Such events on the inner shelf are not consistently predictable using current observations farther offshore over the mid-shelf (100-200 m water depths).
3. Residence times of pollutants and passive larvae in the upper waters of the western Santa Barbara Channel are shorter when topographic Rossby modes are present. The modes are an important factor in controlling the stability of the cyclonic circulation in the channel; when present they disrupt this circulation.

The operational goal of putting real-time data from the HF radar network onto the internet was accomplished. Near real-time current observations from the array shown in Fig. 1 are available at http://www.icess.ucsb.edu/iog/codar_realtime.htm.

STUDY PRODUCTS:

Publications:

Beckenbach, E. H. (2004). "Surface circulation in the Santa Barbara Channel: An application of high frequency radar for descriptive physical oceanography of the coastal ocean". Ph.D. Dissertation, Interdepartmental Program in Marine Science. University of California, Santa Barbara**,** pp 126.

Beckenbach, E. H. and L. Washburn (2004) "Low frequency waves in the Santa Barbara Channel observed using high frequency radar", in press, Journal of Geophysical Research.

Cudaback, C. N., L. Washburn and E. P. Dever (2004) "Inner shelf circulation near Point Conception, California", Continental Shelf Research, submitted.

Emery, B. M., L. Washburn and J. Harlan (2004) "Evaluating CODAR high frequency radars for measuring surface currents: observations in the Santa Barbara Channel", Journal of Atmospheric and Oceanic Technology, submitted.

Nishimoto, M. M. and L. Washburn (2002) "Patterns of coastal eddy circulation and abundance of pelagic juvenile fish in the Santa Barbara Channel, California, USA", Marine Ecological Progress Series, 241, 183-199.

Research Presentations:

2001 "Surface circulation on the South-central coast: Mechanisms for larval transport and retention", seminar in the Dept. of Atmospheric Science, UCLA, 24 January.

2001 "Variability in mesoscale oceanographic processes corresponds to variability in the distribution and abundance of rockfish (sebastes spp.) juveniles", Schroeder, D M , M.M. Nishimoto, and L. Washburn, American Society of Limnology and Oceanography, Albuquerque2001, Albuquerque, NM, 12-16 February.

2001 "The physical environment of the Santa Barbara Channel", seminar presented to volunteers of the Channel Islands National Marine Sanctuary", Chase Palm Park, 1 March.

2002 “Observations of Wavelike Phenomena in the Santa Barbara Channel Using HF Radar”, Beckenbach, E.H. and L. Washburn, Ocean Sciences Meeting, Honolulu, HI, 11-15 Feb.

2002 “An Observational Network for Multidisciplinary Time Series on the Central California Coast”, Washburn, L., S. Gaines, E. P. Dever, and D. Reed, Ocean Sciences Meeting February, Honolulu, HI, 11-15 Feb.

2002 “Observations of Wavelike Phenomena in the Santa Barbara Channel Using HF Radar”, Beckenbach, E.H., and L. Washburn, Eastern Pacific Ocean Conference, Stanford Sierra Camp, Fallen Leaf Lake 23-26 Sept.

2002 “How Accurate are Total Vector Surface Currents from a Single HF Radar Site?”, Emery, B. M., L. Washburn, J.A. Harlan, Ocean Sciences Meeting February, Honolulu, HI, 11-15 Feb.

2002 “Circulation near Pt. Conception California”, Cudaback, C., and L. Washburn, PISCO Symposium, Monterey, CA, 10 March.

2002 “An Examination of Small-Scale Coastal Eddies and Pollution Hazards off California Using an Integrated Multi-Sensor/In-Situ Approach”, by P. M. DiGiacomo, B. Holt, and L. Washburn, AIRSAR Workshop, Jet Propulsion Laboratory, Pasadena, CA, 5 March.

2002 “High frequency sampling of nearshore coastal circulation and invertebrate settlement near Santa Barbara California”, C. Cudaback, L. Washburn, J. Caselle, C. Blanchette, B. Gaylord, Eastern Pacific Ocean Conference, Timberline Lodge, OR, 25-28 Sept.

2002 “A coastal observing system on the South-Central Coast for understanding links between the regional circulation, pollutant transport, and dispersion, L. Washburn, D. Reed, C. Ohlmann, C. Cudaback, E. Dever, California and the World Ocean, Santa Barbara, CA, 27-30 Oct.

2002 “Inner-Shelf Circulation Near Point Conception, California”, Cudaback, C., L. Washburn, E..P. DeverOcean Sciences Meeting February, Honolulu, HI, 11-15 Feb.

2002 “How does the ocean flow in the Santa Barbara Channel?”, Geography Awareness Week presentation to Sue Bupperts and 2 other 5th class, Adams School, 18 November.

2002 “How does the ocean flow in the Santa Barbara Channel?”, Geography Awareness Week presentation to 5th classes of Steve Bergdahl and Jennifer Edmonston, Adams School, 26 November.

2002 “Pollution Hazards Off the Southern California Coast: Satellite and In Situ Observations of Naturally Occurring Oil Seepage, Storm Water Runoff and Wastewater Plumes. Water Quality: Ocean Modeling, Observations and Remote Sensing”, P. M. DiGiacomo,

B. Holt, and L. Washburn, California and the World Ocean, Santa Barbara, CA, 27-30 Oct.

2003 "Vorticity, divergence, and flow states in the western Santa Barbara Channel", Beckenbach, E.H., and L. Washburn, Eastern Pacific Ocean Conference, Wrigley Institute, Catalina Island, 24-27 Sept.

2003 "Low-frequency dynamics and nutrient flux to the inner shelf of the Santa Barbara Channel", E. McPhee-Shaw, L. Washburn, and D. Siegel,Eastern Pacific Ocean Conference, Wrigley Institute, Catalina Island, 24-27 Sept.

2003 "Sub-mesoscale eddies along the northern Santa Barbara Channel: A possible mechanism for nutrient delivery to the inner shelf", Bassin, C.J., L. Washburn, and E.E. McPhee-Shaw, Eastern Pacific Ocean Conference, Wrigley Institute, Catalina Island, 24-27 Sept.

2003 "An Update on the Regional Ocean Observing Systems along the US West Coast", Barth, J., A. Baptista, M. Kosro, D. Martin and J. Newton, L. Rosenfeld, F. Chavez, M. McManus and M. McNutt, E. Terrill and L. Washburn , T. Garfield, J. Hunter, Eastern Pacific Ocean Conference, Wrigley Institute, Catalina Island, 24-27 Sept.

FINAL STUDY REPORT

Summary

A three-year record of high frequency (HF) radar observations of surface currents in the western Santa Barbara Channel (SBC) reveals sequences of alternating cyclonic and anticyclonic vortices propagating westward with a period of about two weeks. The sequences last up to a few months and occur intermittently throughout the year. The surface velocity distribution of cyclones and anticyclones are anti-symmetric with a mean propagation speed of ~5 km day^{-1} and relative vorticity magnitudes $|\zeta|$ of order 0.1 f, where f is the local Coriolis parameter. The Coriolis parameter quantifies the effect of the earth's rotation with latitude. The value of $|\zeta|/f = 0.1$ indicates that the earth's rotation is important the dynamics of the vortices. These propagating vortices resemble the propagating cyclones in the 10-25 day pass-band reported in the SBC by Harms and Winant (1998).

Complex empirical orthogonal function (CEOF) decomposition in the 10-20 day pass-band, following the method of Wallace (1972) for detecting propagating features, partitions variance into two dominant modes. The first mode with an average period of 14.4 days explains 45% of the velocity variance and represents the alternating cyclones and anticyclones that are evident in the band-pass filtered record. The second mode, with an average period of 13.3 days, explains 25% of the velocity variance and mainly represents alongshore fluctuations. Amplitude functions of the two modes correlate with *in situ* current time series at 5 and 45 m depths obtained from moorings at the east and west channel entrances suggesting coupling between the modes and the larger-scale circulation of the northern Southern California Bight.

Auad and Henderschott (1997), Auad et al. (1999) investigated the relationship between low-frequency flow in the 6 - 18 day band and forcing by wind stress and remote adjusted sea level. The remotely-forced flow was explained as a coastal trapped, low-mode hybrid-wave with characteristics of both Rossby and Kelvin waves. The higher spatial resolution HF radar observations support this interpretation since the period and along-shore flow of mode 2 are consistent with a coastal trapped wave.

We hypothesize that mode 1 is a resonant response of the Santa Barbara Basin in the form of a trapped topographic Rossby mode (TRM). A harmonic stream function representation of the spatial mode resembles the predicted pattern based on a simplified analytical model of a fundamental TRM in a closed basin. Peak relative vorticities over the basin are about a factor of four higher than over the edges, indicating topographic control. The amplitude of mode 1 is consistently large when the frequency difference between modes 1 and 2 is small. This suggests that the propagating vortices of mode 1 are a basin-scale resonant response to the coastal trapped wave represented by mode 2.

1. Background

The coastal ocean supports diverse circulation patterns due to the imposition of the coastal boundary and sloping topography. Along straight coastlines, coastal upwelling Sverdrup (1938) and coastally trapped-waves (CTWs) including barotropic Kelvin and topographic-Rossby modes are well known examples with straight-forward analytical descriptions Brink (1991). Real coastlines can be irregular with complex offshore topography and, in the presence of stratification, 3-dimensional fluid structures are common including jets, eddies, fronts and a series of baroclinic Kelvin and Rossby waves. The Santa Barbara Channel (SBC) is an example of a coastal region with variable bottom slope, offshore islands, and a deep basin, the Santa Barbara Basin (SBB). The SBC, located at the northern end of the Southern California Bight (SCB), runs east to west approximately 100 km between Pt. Mugu and Pt. Conception. The Northern Channel Islands of Anacapa, Santa Cruz, Santa Rosa and San Miguel form the Channel's southern boundary. The 40 km wide channel is a region where coastal circulation patterns are complicated by irregular topography, interacting water masses and strong wind stress forcing.

Circulation patterns in the SBC were first assessed by Kolpack (1971) based on hydrographic surveys conducted during 1969 and 1970 in response to the Santa Barbara Channel oil spill of 1969. Drifter cards released during these surveys revealed that a complex field of eddies prevailed in the eastern channel, positioned between a large persistent cyclonic cell in the western channel and northwest flow at the eastern entrance. Later research conducted during the Organization of Persistent Upwelling Systems (OPUS) project and the Santa Barbara Channel Circulation Study (1983-1984) examined local flow patterns in response to the frequent, vigorous wind forcing common in the western channel. Brink (1983), Huyer (1983), Winant et al. (1987) found that near Pt. Conception and to the north flow responds to alongshore wind stress following classical Ekman dynamics and the thermal wind relationship. In contrast, Atkinson et al. (1986), Brink and Muench (1986), Barth and Brink (1987) described flow within the SBC as a complex system of eddies, jets, and fronts with poor correlation to local wind forcing. More recently, several studies have described flow in the SBC as a sequence of synoptic states consisting of upwelling/relaxation and cyclonic regimes regulated through a momentum balance including significant contributions from wind stress, wind stress curl, sea level tilt and Coriolis terms Auad and Henderschott (1997), Harms and Winant (1998), Oey (1999), Winant et al. (1999), Oey et al. (2001).

An additional circulation pattern observed by Harms and Winant (1998) within the SBC is that of "propagating cyclones". They observed that AVHRR satellite images often indicate cyclonic eddies drifting westward with a period of approximately 14 days. As one cyclonic eddy approached the western entrance, another appeared north of the western tip of Santa Cruz Island. These features extended below the thermocline based on observation from an array of vector measuring current meters (VMCMs) at depths of 5 and 45 meters placed around the SBB. Within the 10 to 25 day band, maximum lagged correlations of longitudinal velocities between neighboring stations indicated a translation rate of 0.06 m s^{-1}.

Auad and Henderschott (1997), Auad et al. (1999) investigated mechanisms of current generation and volume transport at the eastern entrance of the SBC in the 6 to 18 day band.

They found significant linear relationships between transport and both local wind stress and remote adjusted sea level (ASL). Regional-scale ASL behavior was consistent with theoretical predictions of a poleward propagating hybrid Kelvin-topographic Rossby wave Brink and Chapman (1985). Their mass-transport time series for the east and west entrances and the inter-island passages of the SBC also exhibited energy peaks at periods near 14 days

In this study, propagating flow features in the 10-20 day band, comparable to the bands identified by Auad and Henderschott (1997), Harms and Winant (1998), are further explored. Using high frequency (HF) radar with coverage over SBB, we have isolated the surface expression of what we hypothesize is a low frequency resonant response of the basin to forcing by CTWs propagating poleward along coast of the Southern California Bight (SCB). The resonant response resembles a barotropic trapped Rossby mode (TRM) similar to the TRMs identified in the Straits of Sicily Pierini (1996) and on the Iceland-Faeroe Ridge Miller et al. (1996).

The propagating eddy patterns within the 10-20 day band do not dominate circulation within the channel, but represent ~15% of the subtidal velocity variance. However these patterns are a curious aspect of the local circulation which may affect other flow regimes. For example, the propagating eddy patterns appear to constructively and destructively interfere with a persistent cyclonic circulation found over the SBB that can retain juvenile fishes Nishimoto and Washburn (2002). In addition, the regions between eddy centers are alternating cross-channel jets which propagate westward along with the vortices and may significantly influence cross-channel advection between the mainland coast and the offshore islands.

2. Observations

Hourly surface current observations from an array of three HF radars from 1 January 1998 through 31 December 2000 are the primary data used in this study. Observations for the period 2001-2003 are consistent with the three year period of this study. The HF radars were direction-finding systems (Coastal Ocean Dynamics Applications Radar or CODAR, manufactured by CODAR Ocean Sensors, Ltd. of Los Altos, CA) operating at ~12 MHz over a range of 42 km with resolution of 1.5 km and azimuthal resolution of 5^{o}. Radial current vectors were available from three radars on the mainland coast (from east to west) at Coal Oil Point (COP), Refugio State Beach (RFG), and Pt. Conception (PTC) (Fig. 1).

Figure 1. Study area showing the Santa Barbara Channel and Santa Barbara Basin. Inset shows study area (shaded box) on California Coast. Color contours show percent coverage from the HF radar array over the

three year study period. HF radar locations at Point Conception (PTC), Refugio (RFG), and Coal Oil Point (COP) are indicated by dots in circles. SAMI, SMIN, SMOF, and AMNI are current meters deployed by the CCS. SMI, SRI, SCI, AMNI and Pt. M. identify San Miguel, Santa Rosa, Santa Cruz, Anacapa Islands, and Pt. Mugu respectively.

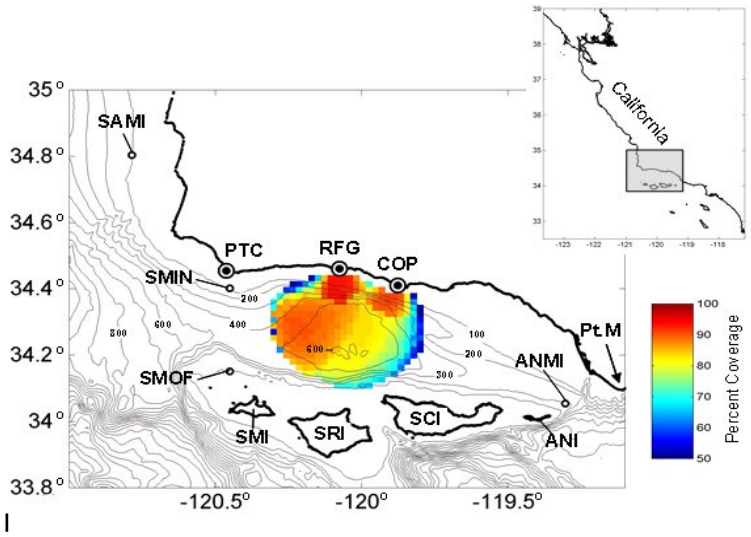

Following Paduan and Rosenfeld (1996), eastward and northward velocity components were computed at points over a 2 km square grid. The grid consists of 360 contiguous points covering 1440 km^2 centered over the SBB. Surface current vectors are calculated from all radial vectors within 3 km of each grid point using the least-squares method of Gurgel (1994).

We subjectively determined the coverage area by attempting to maximize the size of the long-term foot print of the HF radar array while minimizing data gaps. Grid points were excluded within 3 km of the coastline to avoid contamination from overland signal returns and avoid the radar baselines. As described in Emery et al. (2004), spatial coverage from each site within the radar footprint varied over a range of time scales due to several factors including failure of the radar algorithms to determine radial currents, broadcast interference, ionospheric propagation, and equipment failures. Surface current vectors are available for a minimum of 50% and maximum of 95% of the three-year record at individual grid points (color contours, Fig. 1). Averaged over all grid points, the velocity time-series over the coverage area is 80% populated. Because our analysis focused on time scales greater than 10 days, only the longer-lasting gaps were a major concern in the analysis. Fortunately, these were infrequent in the record, particularly in 1998 and 1999.

Data from long-term moorings, maintained by the Center for Coastal Studies (CCS) at the Scripps Institution of Oceanography, place the higher spatial resolution HF radar observations in a larger spatial context and provide sub-surface observations. Four moorings (Anacapa Middle, ANMI; San Miguel Inshore, SMIN; San Miguel Offshore, SMOF; and Point Sal Middle, SAMI) with vector measuring current meters (VMCMs) at 5m and 45m depths provided velocity measurements every 4 minutes at the east and west entrances and north of Pt. Conception (Fig. 1). Hourly, quality-controlled data were made available to us by CCS. Data concurrent with the HF radar time series were available through 19 November 1999 and

13 August 2000 for the 45 meter and 5 meter VMCMs, respectively. Harms and Winant (1998), Hendershott and Winant (1996), and Chen and Wang (1999) describe the mooring data in detail.

3. Methods

We used several data processing steps to characterize narrowband wave-like circulation patterns. Data gaps were filled, the frequency band containing the wave-like motions was identified, and the time series were filtered to isolate the relevant frequency band. The time series were then decimated to one observation per day. Relative vorticity ζ proved useful in quantifying the propagating vortices because of their strong rotation. We computed hourly estimates of ζ at grid points using centered first differences at points inside the coverage footprint (i.e. only at points where total velocity vectors were available at the four adjacent points). ζ estimates were normalized relative to planetary vorticity f ($8.2 \times 10^{-5} s^{-1}$ at 34.25º N). Some basic characteristics of the propagating vortices, such as length scales and period, were determined by examining the filtered time series. Then complex empirical orthogonal function (CEOF) decomposition was used to quantify the strength of the dominant flow patterns. Stream function estimates of the dominant modes were used for flow visualization and for comparison of the propagating vortices with an analytical TRM model.

3.1 Missing Data

Gaps occurred in all of the time series: 19.5% were missing over the 3-year record of HF radar data; 12.6% were missing for the 5 m moored current data records; and 13.2% were missing for the 45m moored records. Because some of the time series analysis methods employed, such as digital filtering and CEOF decomposition, required complete time series, it was necessary to estimate missing portions of the data records. We assumed (and verified) that the velocity observations were sampled from a multivariate normal distribution. Missing observations were optimally estimated using maximum likelihood principles as described by Orchard and Woodbury (1972) and Beale and Little (1975).

This method is a two-step, iterative multiple linear regression procedure. One step is parameter estimation of the data's underlying probability distribution conditioned on the observed data and the prior estimates of the missing data. The other step updates estimates of missing values by regression on the observed values using the estimated distribution parameters, in this case the mean vector and covariance matrix. The procedure starts on either step with some sensible initial estimates of the missing values or the distribution parameters and continues until convergence within a chosen tolerance is met. More details on the procedure are provided by Beckenbach (2004), Beckenbach and Washburn (2004).

3.2 Frequency band selection and filtering

Previous studies of low-frequency flow in the SBC have focused on the 10-25 day band Harms and Winant (1998) and the 6-18 day band Auad and Henderschott (1997). We identified westward propagating features within the overlapping 10-20 day band by computing the squared coherence γ^2 for time series of ζ along the SBC axis as discussed below in section 4. To further examine the flow in this band, we digitally filtered the surface current time series in two steps using MATLAB numerical routines. The two-step filtering process was necessary because the pass-band frequency range (0.05-0.1 cycles per day, cpd) was a small fraction ($1/600^{th}$) of the total bandwidth (0-12 cpd). First, a fifth order Butterworth low-pass filter with a half-power cutoff corresponding to a 36 hr period was applied to the hourly velocity time series and the data were decimated to one point per day. Second, the decimated data were band-pass filtered to retain periods between 10 and 20 days using a ninth order Type II Chebyshev filter with ripple peaks of –40 db relative to the passband. Both filters were applied in the forward and reverse directions to eliminate phase shifts.

3.3 Complex empirical orthogonal function analysis

Once the current time series were filtered to eliminate variance outside of the 10-20 day band, we computed complex empirical orthogonal functions (CEOFs) following the method of Wallace (1972) to evaluate the spatial patterns and temporal evolution of the dominant modes of variability. Auad and Henderschott (1997) used the technique to examine low frequency coastal waves propagating through the SBC based on moored current and bottom pressure time series. They also present a succinct description of the method. In the CEOF procedure each time series (u and v are treated independently as scalars) is augmented with an imaginary component to provide phase information to enable detection of variance propagation through the array.

CEOFs differ from the more conventional real-EOFs because the associated eigenvalue problem is based on the band-averaged cross-spectrum matrix rather than the standard data covariance matrix. With real-EOFs propagating features can be spread across several modes, obscuring their detection. With narrow-banded CEOFs, propagating modes are distinct and uncorrelated across a finite frequency band. We argue that the two dominant CEOFs found in the 10-20 day band represent distinct propagating waves, although no such dynamical interpretation is implied by the CEOF method which is purely statistical.

3.4 Stream Function Estimation

The stream functions Ψ was used to estimate dynamic topography associated with surface flow patterns and to compare these results with a simple theoretical model. An estimate of the nondivergent flow field, recovered by differentiation of the streamfunction, is a useful first-order characterization of the circulation patterns. The residual velocity fields contain the corresponding divergent component of circulation. Ψ was computed using harmonic expansions as described by Auad et al. (1998), Dever et al. (1998). The expansions were estimated by minimization of the square of the difference in the u (eastward) and v (northward) velocity components between velocity observations and non-divergent velocities based on the derivatives of Ψ. A similar method was used by Vastano and Reid (1985) with

two-dimensional (2-D) half-range sine expansions with constant Ψ on the domain boundaries. Auad et al. (1998), Dever et al. (1998) used the approach on a boundary-fitted orthogonal coordinate system for arbitrary Ψ along open lateral boundaries with explicit boundary conditions imposed for the alongshore boundaries. When open boundaries circumscribe the domain, as in this analysis, 2-D Fourier basis functions with arbitrary phase can be used to avoid edge constraints. Stream function contours are scaled as $\eta = \Psi f/g$ to approximate changes in sea surface elevation.

4. Results

4.1 Propagating Rotary Flows

Preliminary analysis of raw hourly surface current patterns from the HF radars revealed westward propagating rotary flow patterns such as those shown in Fig. 2. The example shows two oppositely rotating eddy-like patterns over the Santa Barbara Basin on 26 May 1999.

Figure 2. Two counter rotating eddies in the coverage area over the Santa Barbara Basin on 16 May 1999 at 0300 GMT. Color contours give ζ/f according to the color scale to the right. The white line identifies the transect used to examine along channel variability of propagation.

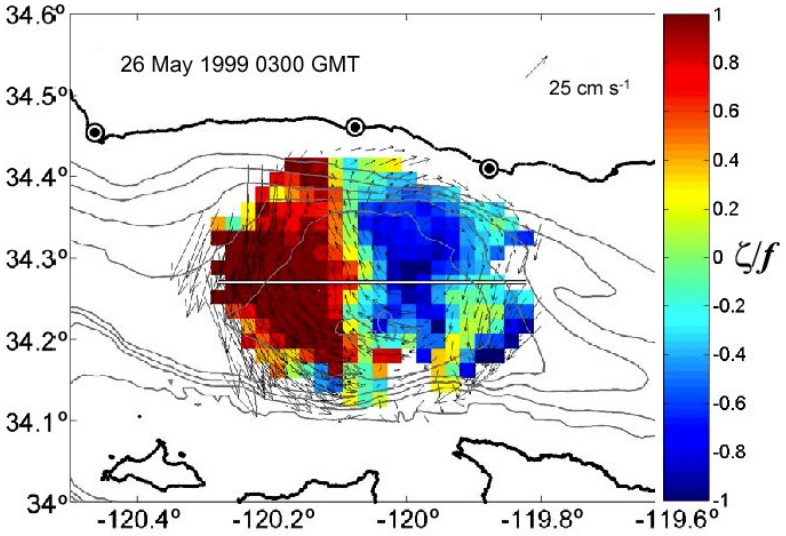

The cyclonic flow pattern on the western boundary of the basin is intensified on its western, southward flowing side with maximum flow speeds of ~0.5 m s^{-1} and ζ/f of order 1. The anti-cyclonic pattern on the northeast side of the basin has lower flow speeds, is more symmetric, and has ζ/f of order -0.6. Both patterns span the north-south extent of the basin with horizontal length scales on the order of the basin width or about 25 km. Sequences of images suggested a westward propagation speed of about 4.7 km d^{-1}. Similar propagating flow patterns at comparable speeds have been found in other circulation studies of the SBC. For example, Harms and Winant (1998) (their Plate 1a) show a westward propagating cyclonic eddy visualized by a sequence of satellite sea surface (SST) images in August 1994.

Typically, energetic flow patterns in the SBC obscure propagating rotary structures like those of Fig. 2. One such pattern is the mean tendency for cyclonic flow in the western SBC as discussed by Harms and Winant (1998), Hendershott and Winant (1996), and Atkinson et al. (1986), Brink and Muench (1986), Auad et al. (1999).

From these HF radar observations we estimate a mean ζ for the three-year record of $0.18f$ over the radar coverage area shown in Fig. 1; maximum observed values averaged over the coverage area are on the order of $0.5f$. Local values exceeding f are observed occasionally as in Fig. 3. Often propagating eddies appear as modulations of the larger cyclonic flow pattern: propagating cyclones temporarily intensify the pattern, propagating anti-cyclones weaken it.

Time-longitude contours for 1999 (Fig. 3a) show the evolution of ζ/f along an east-west transect down the channel axis (transect shown in Fig. 2) calculated using the filled-in hourly time series with no filtering. Coherent rotational features, mostly cyclonic, at scales approaching the basin width appear as continuous, nearly vertical bands. The dashed vertical line of Fig. 3 identifies the time of the vortex pattern of Fig. 2. The flow varies on timescales of days to weeks over the basin, but a tendency for cyclonic flow (red-biased contours) is evident.

Figure 3. a) Time-longitude contours of ζ/f computed from hourly HF radar observations along transect shown in Fig. 3 for 1999. **b)** as in panel a) but with ζ/f low-pass filtered with a cutoff frequency of 1/36 hours^{-1}. **c)** as in panel a) but with ζ/f band-pass filtered with cutoff frequencies (1/10) days^{-1} to (1/20) days^{-1}. Dashed vertical line indicates time of velocity pattern of Fig. 3. Color scales at right in each panel indicate values of ζ/f.

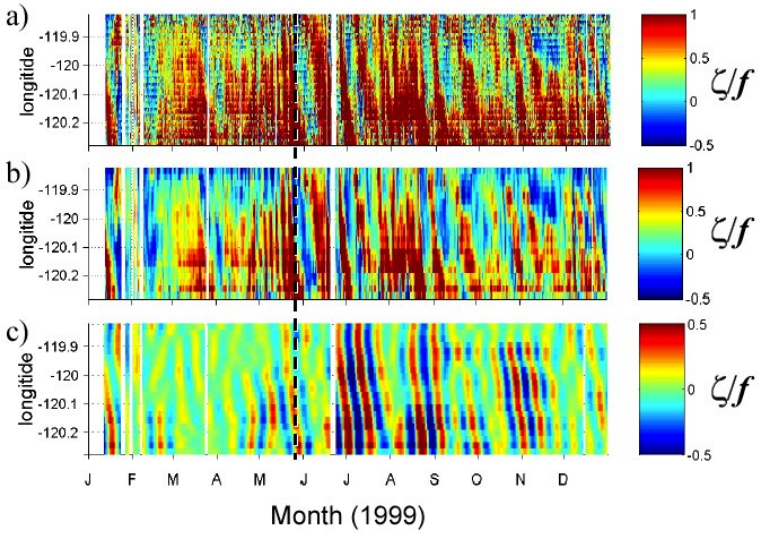

Periods of negative vorticity (blue-biased contours) lasting up to a few weeks also occur, particularly along the transect's eastern portion. A general negative sloping of the contours indicates persistent westward propagation of cyclonic and anti-cyclonic vorticity features along the SBC axis. Low pass filtering of the time series (cutoff frequency of 1/36 hr^{-1}) more clearly shows the westward propagation by removing variance at tidal and higher frequencies (Fig 3b) It also clarifies the occurrence of negative vorticity, particularly on the eastern portion of the transect.

To identify the dominant time scales associated with westward propagation, we computed the squared coherence, γ^2, and phase difference, ϕ, between vorticity time series at the transect endpoints. A peak in γ^2 between 0.05-0.1 cpd indicates significant coherence (95% confidence threshold) for periods of 10-20 days (Fig. 4). The γ^2 peak of 0.5 corresponds to a period of approximately 15 days. ϕ in the 10-20 day band ranges from 195-240^o with the peak corresponding to 210^o. The positive ϕ of 210° indicates that vorticity at the east end of the transect leads the west end by about nine days, consistent with the westward propagation inferred from Fig. 3. The distance between the ends is 42 km so the implied westward propagation speed is ~ 4.7 km d^{-1}.

Figure 4. a) Squared coherence γ^2 and **b)** phase φ of ζ between the ends of the transect shown in Fig. 2. Dashed lines indicate the frequency band 1/10 day^{-1} to 1/20 day^{-1} over which γ^2 is significant. Dotted lines shows 95% significance threshold.

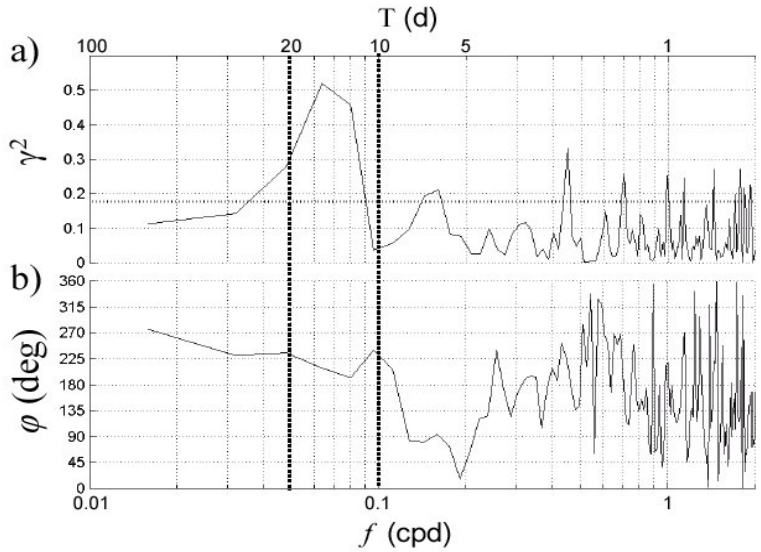

Based on the γ^2 peak, velocity data were band-pass filtered to remove variance outside the 10-20 day pass band. Contours of ζ/f in the pass band show distinct alternating stripes which represent trains of counter-rotating features (Fig. 2c). This banding suggests a channel-scale instability or wave phenomenon.

Figure 5. a) Longitude-time contours of ζ/f for 21 June to 21 July 1999. Color scale for the contours is given at the bottom. **b)** Surface velocity patterns at times indicated by horizontal lines in panel a). Sloping red (blue) line connects centers of cyclones (anti-cyclones) every three days. Arrow at lower left in each velocity pattern indicates 10 cm s^{-1}. All data have been band pass filtered to retain frequencies from 1/10 day^{-1} to 1/20 day^{-1}.

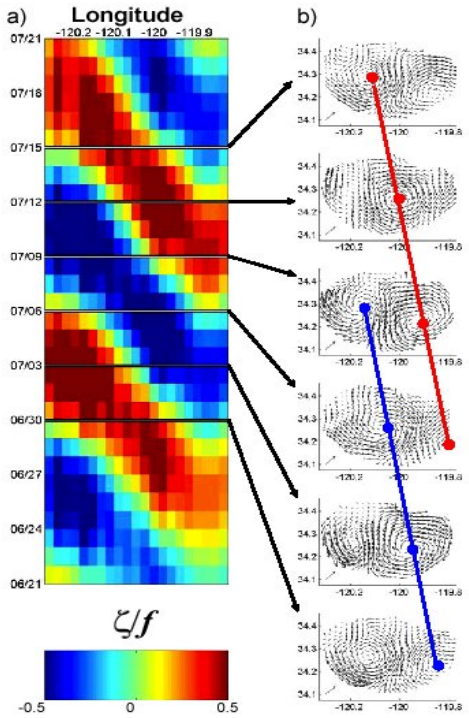

The correspondence between the red and blue stripes and propagating cyclonic and anti-cyclonic vortices is apparent when the stripes are compared with patterns of band-pass filtered velocity vectors (Fig. 5). During the period 21 June – 21 July 1999 alternating anti-cyclonic and cyclonic vortices move through the coverage area. The propagating pattern varies strongly but recurs over the 3-year record with vortex trains lasting up to a few months.

Vorticity time series along the transect reveals that the radar footprint is often too small for observing the complete evolution of the propagating features. Some of the stripes in Fig. 3c are cut off at both ends, although this occurs more frequently at the west end of the transect. There are no periods during which the HF radar coverage extended farther east so investigation into an eastward origin is precluded. During May - October 1998 coverage extended an additional 12 km to 120.4º W, over the western sill of the basin. We used data from this area to examine the evolution of the vortices as they propagate over the sill. Other periods of continuous coverage over this area were too short for analysis at periods of 10-20 days.

ζ/f contours over the extended coverage area show a marked decrease in relative vorticity as the vortices propagate westward over the western sill (Fig. 6a). Some propagating variance in the 10-20 day band persists over the sill such as in late June and early July 1998.

Figure 6. a) Longitude-time contours of ζ/f for 1 June – 1 September 1998 along extended transect (see text). Color scale for ζ/f is given at right. **b)** Solid line (left scale) shows average of envelope of amplitude ζ/f profile between 15 June – 15 August 1998. This time period is shown by dotted lines, panel a). Dashed line (right scale) shows bottom contour along transect of Fig. 2.

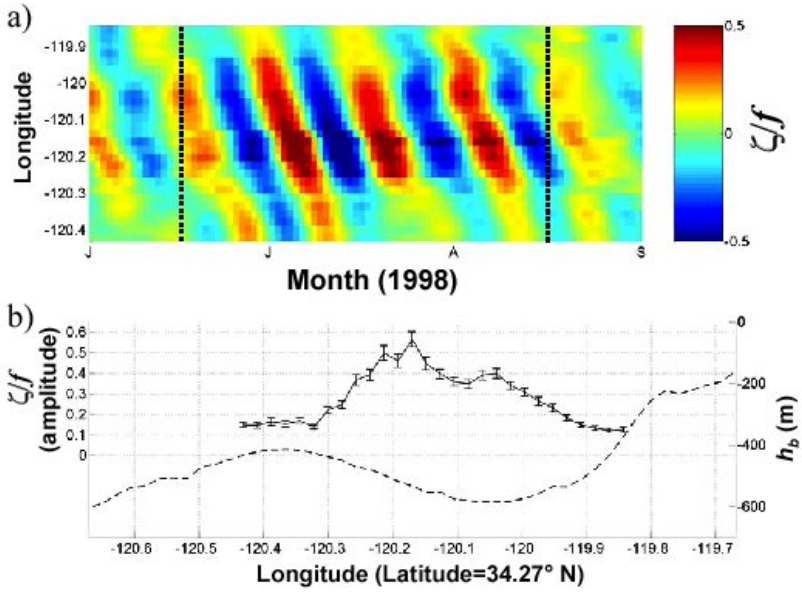

Shading of the contours indicates that the largest values of ζ/f are found near 120.2° W, above the slope leading to the western sill. Then the amplitude of ζ/f fluctuations decreases rapidly over the upper slope and remains small over the sill. This is confirmed in a comparison of the average envelope of ζ/f and the bathymetric profile along 34.27° N (dashed line, Fig. 6b). The amplitude envelope of ζ/f averaged over the 15 June – 15 August 1998 interval, shown by the dotted bars in Fig. 6a, increases from 0.11 on the eastern end of coverage area to a peak of 0.55 at 120.17° W. West of the peak it decreases rapidly to about 0.15 over the sill itself. A similar reduction in ζ/f amplitude at the ends of the transect were indicated for the entire 3-year record but the trend was not as well resolved due to the limited westward extent of the transect.

The pattern of striped contours in Fig.6a and the eddy velocity patterns of Fig. 5b suggest symmetry between the cyclonic and anticyclonic features. We quantified this symmetry by conditionally averaging numerous cyclones together and numerous anti-cyclones together at similar phases during their propagation. To estimate the velocity field of the propagating cyclones, all times over the 3-year band-pass filtered record were identified which had maxima of $\zeta/f > 0.2$ at a point near the center of the SBB (circle, Fig. 7a). A total of 32 maxima satisfied this condition. At these times fully developed cyclones occupied the central portion of the basin. Then for each grid point at these times the velocity components, u and v, were individually averaged. The resulting pattern is shown as black arrows in Fig. 7a. A similar procedure for anti-cyclones found 35 peaks with $\zeta/f < -0.2$. Velocity components -u and -v for the anti-cyclones are shown as gray arrows in Fig. 7a. Together these cyclones and anticyclones account for the upper 45% of $|\zeta/f|$ for the 3-year record. Strong spatial correlation among the vectors ($\rho = -0.998$; $r^2 = 0.995$) indicates the high degree of anti-symmetry between the mean velocity fields of the cyclones and anti-cyclones over most of the

coverage area. Large differences in current direction only occur over the western sill where velocity vectors are small.

Because of the symmetry between the cyclones and anti-cyclones and their radial similarity, we computed representative radial profiles of tangential velocity, $v_t(r)$, and radial velocity, $v_t(r)$, where r is the distance from the center of the velocity patterns (plus signs (+) in Fig. 7a and 7b).

Figure 7. a) Black arrows show conditionally averaged cyclonic velocity pattern and gray arrows show conditionally averaged anti-cyclonic velocity pattern. Velocity components of anti-cyclonic pattern have been multiplied by -1 for comparison. Patterns are formed by averaging velocity fields together subject to the conditions: (1) local maxima (for cyclones) and minima (for anti-cyclones) occur at the location indicated by the black circle; and (2) these maxima and minima satisfy $|\zeta|/f > 0.2$. Velocity scale at lower left. **b)** Cyclonic velocity from CEOF mode 1 for phase $\varphi_{A1} = 221°$. In both panels, dotted circle indicates area, with center at plus (+) sign, used to produce the radial distributions of Fig. 8.

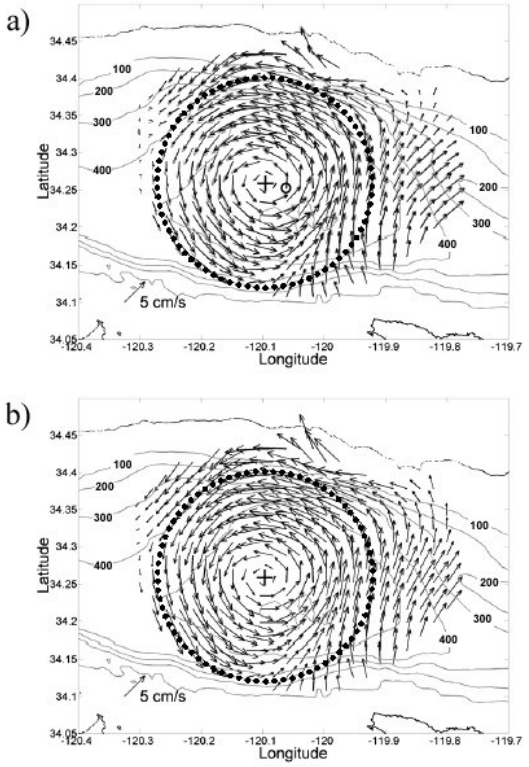

We used the mean velocity patterns of Fig. 7a with cyclones combined with Stoke's theorem and the divergence theorem applied to a circular area were used to calculate the tangential velocity component $v_t(r)$ and the radial component $v_r(r)$ as functions of radius from the center of the eddies. The circular area was centered on the mean eddy center (plus sign (+), Fig. 7a). Also computed were the radial distributions of $\zeta(r)$ and the horizontal divergence, div v(r). Tangential and radial velocities at the eddy center were assumed to be zero. Profiles of $v_t(r)$ and $v_r(r)$ are linearly related (r^2=0.97), increasing from zero at the eddy center (extrapolating) to maximal values at ~10 km (Figures 8a and 8b). Signs are opposite with positive $v_t(r)$, representing cyclonic circulation, associated with negative $v_r(r)$, representing convergent flow towards the eddy center. The profile of $v_t(r)$ increases from ~2 cm s^{-1} at 2 km radius to a

maximum of ~7 cm s^{-1} at 10 km before decreasing to 5-6 cm s^{-1} at 16 km (Fig. 8a). The $v_r(r)$ profile is negative everywhere, lying in the range -0.5 to -1.5 cm s^{-1} (Fig. 8b). Radial profiles of $\zeta(r)/f$ and div v(r) are similarly related (Figures 8c and 8d). Extreme values of opposite sign, 0.28 for $\zeta(r)/f$ and -4.1×10^{-6} s^{-1} for div v(r), occur at the cyclone center and transition monotonically towards zero at 16 km, on the outer edge. Anti-cyclonic flow (negative $v_t(r)$ and $\zeta(r)/f$) is associated with divergence (positive $v_r(r)$ and div v(r)) and is represented by scaling the radial profiles of Fig. 8 by a factor of -1.

Figure 8. Mean radial distributions of **a)** tangential velocity, $v_t(r)$, **b)** radial velocity, $v_r(r)$, **c)** normalized vorticity, $\zeta(r)/f$, and **d)** divergence, div v. Solid lines are averages based on conditionally averaged patterns of Fig. 7a and dashed lines are based on CEOF mode 1 pattern of Fig. 7b. Scatter about the profiles are point calculations based on the CEOF mode 1 pattern. The scatter represents variability arising due to departure of the mean distribution from radial symmetry.

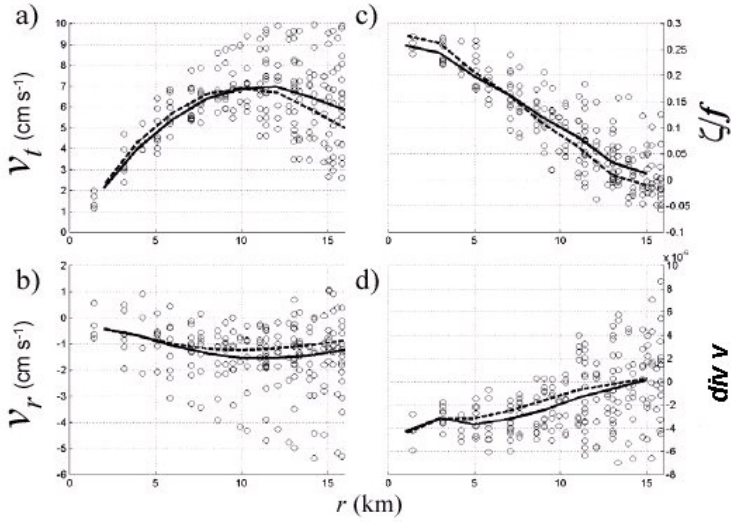

4.2 Modes of variance over the Santa Barbara Basin

Time-longitude contours of ζ/f (Fig. 3) and the time series of velocity distributions (Fig. 5) suggest that trains of westward propagating cyclones and anti-cyclones are common over the SBB. We employed CEOFs to isolate two modes of propagating variance associated with the time-scales of these motions and then explored the relationship between the modes.

The first two CEOF modes account for 45% and 20% the velocity variance in the 10-20 day band, respectively. The spatial structure of mode 1 is similar to the trains of cyclones and anti-cyclones as is seen by comparing the mean velocity field of the cyclones (Fig. 7a) with the velocity field of mode 1 at phase angle $\varphi_{A1} = 221^o$ (Fig. 8b).

Westward propagation of cyclones and anti-cyclones over the SBB is evident over one complete cycle of mode 1 as shown in Fig. 9a. As φ_{A1} progresses from 0 through $\pi/2$, an anti-cyclonic eddy translates westward and a cyclonic eddy enters the eastern edge of the coverage. At π the cyclonic eddy occupies the center of the basin; only a hint of the original anti-cyclonic eddy remains to the west. This sequence resembles the time series of velocity

patterns of Fig. 5b. Stream function distributions scaled as η (Fig. 9a) indicate that the propagating eddies span the basin. Accompanying sea surface elevation differences between centers of the cyclones and anti-cyclones are on the order of 5 mm over separation distances of approximately 30 km.

A strong correspondence exists between ζ/f in the 10-20 day band (Fig. 11a) and the amplitude of the first mode $|A_1(t)|$ (black line, Fig. 11b) over the 3-year record. Gaps in coverage appear as white vertical bands in Fig. 11a. Curves of the first and second mode amplitude functions $|A_1(t)|$ and $|A_2(t)|$ are continuous in Fig. 11b because data were filled using the technique described in Section 3. Large peaks in $|A_1(t)|$ occur from June 1998 through January 1999 and from June through August 1999 (Fig. 3c) when striped vorticity contours are prominent. Mode 1 is relatively weak in winter and early spring 1998 and 1999 and throughout 2000. φ_{A1} increases steadily over the record with an average frequency $\langle f_1 \rangle = 0.069 \pm 0.010$ cpd corresponding to an average period of $T_1 = 14.3$ d (Fig. 11c) with the given frequency envelope defined as ±1 standard deviation of the instantaneous frequency. Angle brackets < > denote a time average.

Figure 9. a) Velocity patterns of CEOF mode 1 at values of phase φ_{A1} shown at left of each panel. Sloping solid (dashed) lines connect centers of cyclones (anticyclones). Velocity scale is at lower left in bottom panel. **b)** As in a), but for CEOF mode 2.

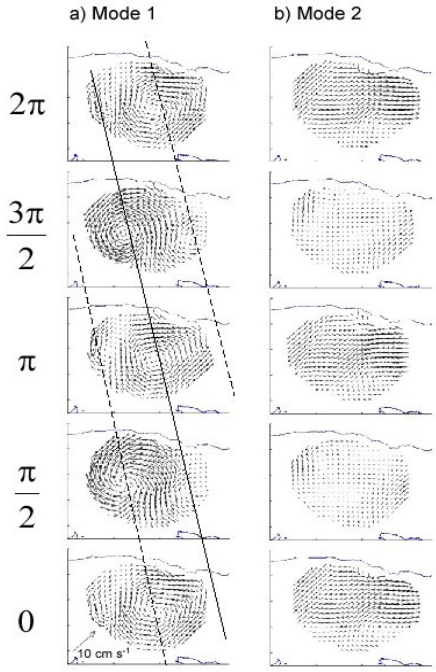

Mode 2, accounting for 20% of variance, exhibits a broad pattern of along-channel velocity fluctuations with much lower ζ than mode 1 (Fig. 9b). The amplitude of mode 2 $|A_2(t)|$ does not show any distinct seasonal trend and is typically smaller than $|A_1(t)|$ (Fig. 11b). Flow for mode 2 is generally eastward and northeastward when $\varphi_{A1} = 0$, westward and southwestward when $\varphi_{A1} = \pi$. Mode 2 has a slightly higher frequency than mode 1 with $\langle f_2 \rangle = 0.075 \pm 0.015$ cpd and mean period $T_2 = 13.3$ d. The mode 2 stream function is a broad pattern of tilting

ηcontours which run diagonally across the channel from southwest to northeast (Fig. 10b). Along the shelf on the northern boundary of the basin they run approximately parallel to isobaths. Further south they cross isobaths. The maximum change in η across the center of the basin is ~ 5 mm. Crowding of η contours indicate highest flow speeds over the northeastern portion of the basin. Spreading η contours over the southwestern region indicates a broadening and weakening flow. Turning of contours near Santa Cruz Island when $\varphi_{A1} = 0$ and π suggests that flow along the island coast is opposite that along the mainland.

Although modes 1 and 2 explain 45% and 20% of the total velocity variance in the 10 – 20 day band, respectively, their spatial distributions are biased such that the modes contribute over 60% of total variance in the regions where each dominates. The spatial distribution of variance indicates that mode 1 explains most of the variance over the basin and the steep slope on the northern edge of the basin while mode 2 explains most of the variance in the northeastern portion of the basin. Combined, the modes explain the most variance, 60 - 80%, over the northern slope of the basin and the least, 20 - 40%, along the southern slope.

Frequency variability based on standard deviations is large compared with differences between the average values of $f_1$and f_2 such that the individual frequency envelopes overlap. Coupling between modes 1 and 2 is suggested by time series of $|A_1(t)|$ and the absolute value of the frequency difference $|\Delta f(t)| = |f_2(t) - \langle f_1 \rangle|$ (Fig. 12). When $|\Delta f(t)|$ is small and exhibits local minima, such as in early December 1998, late March and early July 1999, $|A_1(t)|$ is large and exhibits local maxima. Conversely, when $|\Delta f(t)|$ exhibits local maxima, such as in mid-November 1998, the end of March and mid-June 1999, $|A_1(t)|$ exhibits local minima.

Figure 10. a) Stream function for CEOF mode 1 corresponding to velocity patterns of Fig. 9a). **b)** As in a) but for CEOF mode 2. Contours indicate sea surface height differences with a contour interval of 0.5 mm. Dashed contours are negative. Black and gray vectors show correlated velocities (see text) at 5m and 45m, respectively, from CCS moorings. Velocity scales are shown on bottom panels. Current vectors at western-most current meter shown (SAMI) are displaced south of the actual mooring location. Fig. 1 shows all mooring locations.

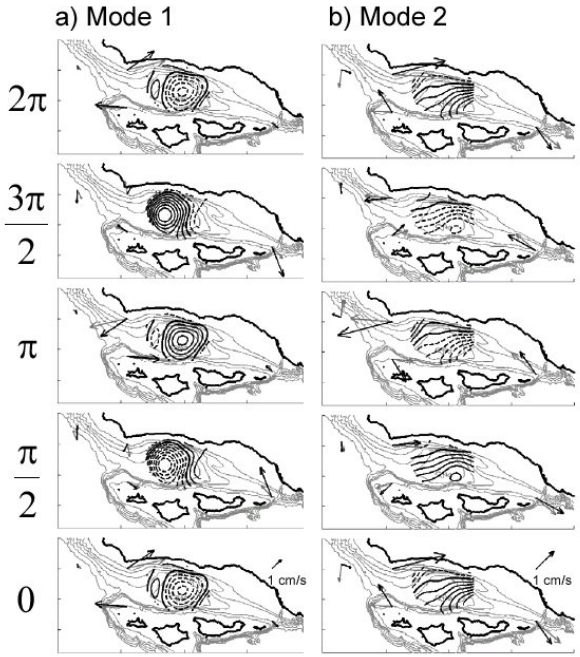

This temporal pattern occurs consistently over the 3-year record, although the amplitudes of maxima and minima in $|A_1(t)|$ are not related to |Δf(t)| in a simple linear way. For example, the peak in $|A_1(t)|$ at the beginning of December 1998 is higher than the peak of early January 1999, even though its |Δf(t)| is larger. Similarly, the trough in $|A_1(t)|$ in late March 1999 is slightly deeper than the trough of mid June 1999, even though its |Δf(t)| is much smaller.

The mean velocity distribution for the cyclonic eddy in Fig. 8a is similar to the first CEOF mode at $\varphi_{A_1} = 221^{o}$ as shown in Fig. 8b. This CEOF distribution was used as the basis for recalculating radial profiles for comparison with those derived from conditional averages. A strength of the CEOF decomposition is the implicit incorporation within each complex mode of the entire time series. Averaging at a single phase angle depends on the continuity of the propagating pattern at all phase angles over all times. In addition, no arbitrary constraints on vorticity magnitude, such as the vorticity threshold used in the conditional averages of Fig. 7, are required to extract the dominant velocity distributions.

Radial distributions of $v_t(r)$, $v_r(r)$, $\zeta(r)/f$, and div v computed from mode 1 are similar to those computed from the mean flow patterns of (Fig. 7a).

Figure 11. **a)** Time-longitude contours for 1998-2000 of ζ/f band pass filtered with cutoff frequencies (1/10) days^{-1} to (1/20) days^{-1}. Color scale as in Fig. 3c. **b)** Time series of CEOF amplitude functions $|A_1|$ (black line) and $|A_2|$ (gray line). **c)** As in b), but for CEOF phase functions φ_{A1} (black line) and φ_{A2} (gray line).

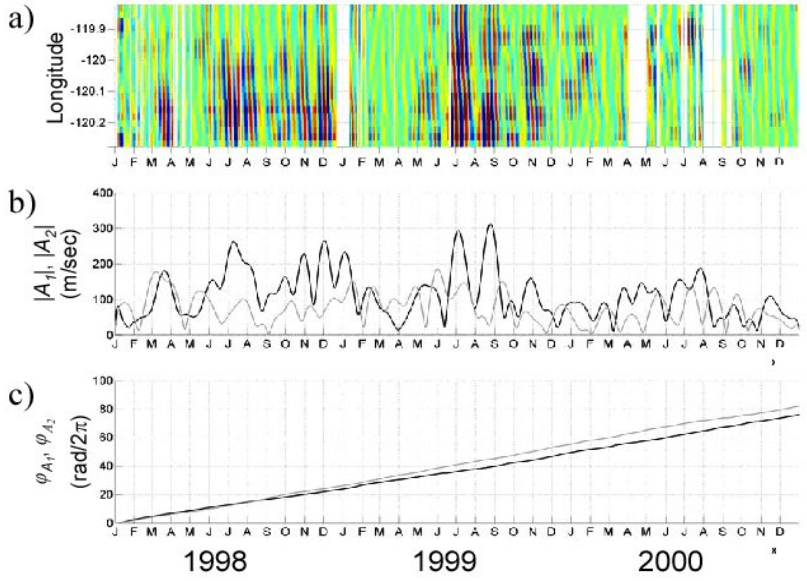

Profiles from mode 1 (solid lines, Fig. 8) correspond to a phase angle of 221º where the correlation with the mean pattern of Fig. 7 was greatest ($r^2 = 0.96$). To produce mean profiles from mode 1, its (non-dimensional) spatial pattern was multiplied by the average magnitude of the upper 45% of values of its temporally-varying amplitude function. The threshold of 45% was chosen to match the upper 45% of ζ/f values used in calculating the mean velocity distribution.

Figure 12. Time series for 1998-2000 of frequency difference magnitude $|\Delta f|$ (black line) and magnitude $|A_1|$ of CEOF mode 1 (gray line).

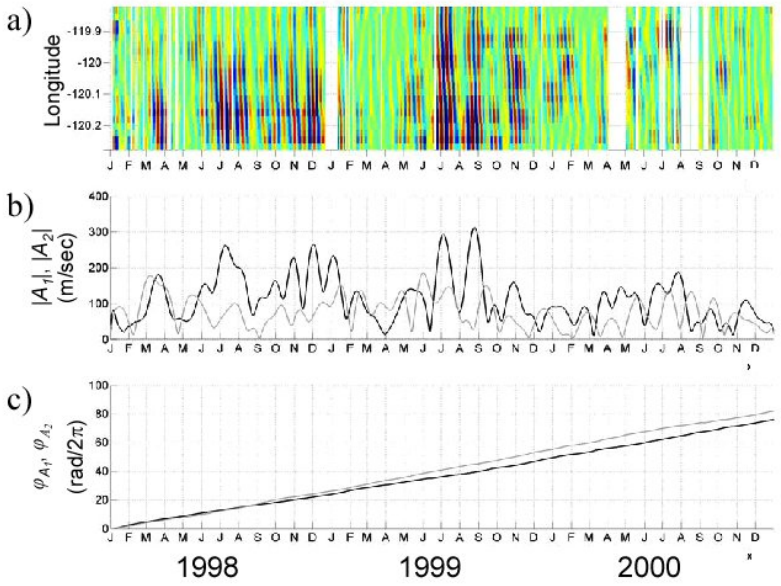

To show variability about the mean radial distributions due to departures from radial symmetry, panels of Fig. 8 include values of each variable at individual grid points as a function of radius based on the CEOF distribution scaling as described above. Scatter in the radial distributions is large, particularly for $v_r(r)$ and div v, although even with the wide range most $v_r(r)$ and div v values are negative.

4.3 Larger-scale current patterns

To explore possible connections between surface flow patterns over the SBB and larger-scale coastal flows we examined the correlation between the CEOF modes and velocity time series from the CCS moorings at the east and west channel entrances. The mooring data were not incorporated into the CEOF analysis because they only overlapped with the HF radar time series for 23 to 32 months. Instead the mooring data were related to the CEOF modes using complex linear regression of the mooring data on the amplitude functions A_1 and A_2. Consistent with the HF radar data, the mooring data were band-pass filtered and augmented with their Hilbert transforms. Complex regression coefficients and associated r^2 values were then calculated.

The resulting moored current patterns are included with the CEOF stream functions in Fig. 10. Currents at SAMI are displaced from their actual position for comparison with the HF radar-derived stream functions. Correspondence between the CEOF modes and correlated mooring patterns is seen for the most widely spaced currents at ANMI and SAMI suggesting that both spatial modes 1 and 2 are related to oscillations of the large-scale alongshore coastal flow, especially to the south but also to the north of Pt. Conception.

The sense of the correlated moored currents agrees with the CEOF spatial distributions. The portion of the currents at ANMI correlated with mode 1 are out of phase with those at SMIN; maximum currents at ANMI occur simultaneously with minimum currents at SMIN and vice-a-versa (Fig. 10a). In contrast, the second mode agrees with ANMI and SMIN in direction and magnitude as may be seen by comparing Figures 9b and 10b. These characteristics suggest that the mode 1 circulation pattern is smaller than the mooring array for mode 1 while the mode 2 pattern is larger. At SMIN and SMOF the alongshore velocity components are approximately opposite in direction with comparable magnitudes. Their phase is consistent with propagation of the weakening (mode 1) eddy patterns over the western sill. With respect to mode 2 (Fig. 10b), flow at SMOF is opposite but reduced in magnitude compared with SMIN. This corresponds well with the reversing of flow seen just north of the Channel Islands, at the southern edge of the HF radar coverage and the expected offshore attenuation in amplitude associated with CTWs. Overall, these results agree with the interpretation of the first mode as a basin response and the second as a coastally-trapped wave.

4.4 Comparison with model results

Evolving patterns of surface currents in the SBC in the 10-20 day band suggests a basin-scale (~30 km) modification of the larger-scale coastal flow associated with poleward-propagating CTWs with wavelengths much larger than the channel scale. Previous studies have shown that CTWs commonly occur along the west-coast of North America, including the SCB and

around Pt. Conception Battisti and Hickey (1984), Davis and Bogden (1989), Hickey (1992), Auad and Henderschott (1997). Auad and Henderschott (1997) observed propagating features in the SBC in the 6-18 day band at longer-than-channel scales which they concluded were hybrid Kelvin-Rossby waves. The second CEOF mode in this study resembles a CTW with surface currents approximately parallel to isobaths along the mainland coast and with an indication of current direction reversal along the slope north of the Northern Channel Islands (Fig. 11b). Auad and Henderschott (1997) found good agreement between a theoretical frequency of 0.073 cpd and an observed period of 0.075 cpd. We found a period for CEOF mode 2 of 0.075 ± 0.005 cpd consistent with these values. The combination of mode 2 and correlated portion of the mooring data (Fig. 11) is also consistent with a broad long-wavelength oscillating flow along the mainland coastal slope.

Mode 1, representing the propagating vortices, is limited horizontally by the basin dimensions (Fig. 7 and 10a). A Rossby wave-like flow is suggested by the symmetry of the cyclonic and anti-cyclonic patterns (Fig. 7a), their frequency, and their westward propagation. The centers of the propagating vortices move westward over the basin at 4.7 km day^{-1} along the channel centerline. This is consistent with topographic control in the north-south direction since the bottom shoals to the north. Topographic control is also indicated by the increase in vorticity over the center of the basin compared with the eastern and western sections of the basin (Fig. 6). In addition, the spatial distribution of variance explained by mode 1 is most significant where the bottom shoals to the north and is much lower over the southern edge of the SBB where the bottom shoals to the south. Over this region the bottom slope does not allow westward propagation of topographic waves.

Figure 13. a) Observed stream function pattern as described by CEOF mode 1 for values of phase φ_{A1} shown at left. **b)** Predicted stream function pattern for the topographic Rossby mode model described by Pedlosky (1987). The similarity of the patterns suggests that the observed propagating eddy patterns are the response of the Santa Barbara Basin to the lowest frequency TRM. The patterns of stream function shown here are similar to those of sea surface elevation with solid lines indicating elevated sea surface and dashed lines indicating lowered sea surface. The darkest contours are zero sea surface elevation.

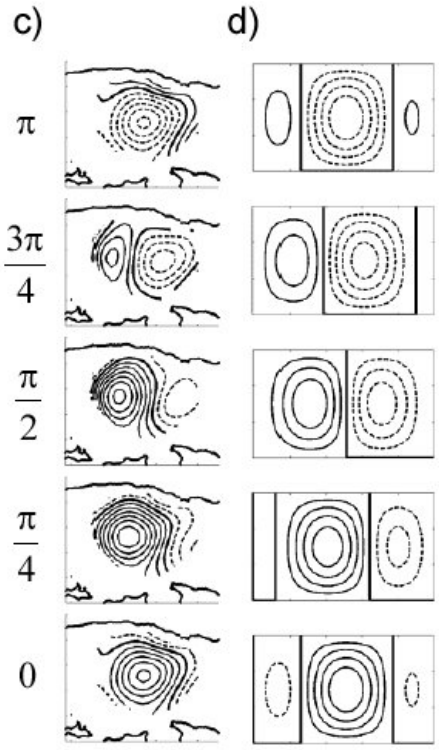

We hypothesize that the mode 1 flow pattern is the lowest frequency topographic Rossby mode (TRM) of the SBB. Observations of TRMs are rare, although they have been observed near Iceland by Miller et al. (1996) and in numerical model outputs of the Mediterranean by Pierini (1996). The conclusion that the mode 1 flow pattern is a TRM follows from the similarity between observed mode 1 velocity patterns and those predicted by an analytical model described by Pedlosky (1987), page 148. Details of the analytical model and its comparison with observations are described in detail by Beckenbach and Washburn (2004). Here just the main results are summarized.

The analytical model assumes that the basin containing a TRM is rectangular with a sloping bottom. The downward slope of the SBB is consistent with the westward propagation of the velocity pattern of mode 1. The dimensions of the SBB and the magnitude of its bottom slope reasonably predict the propagation speed of the eddies along with their dimensions and frequency. This may be seen by comparing the observed streamline patterns of Fig. 13a with the model predictions of Fig. 13. Differences in the patterns may result from the fact that the SBB is circular while the model assumes a rectangular basin. Nevertheless the similarity in the patterns is striking.

5. Conclusions

This study supports the following conclusions:
1. The stability of the predominant cyclonic circulation in the Santa Barbara Channel is strongly affected by the presence of trains of propagating eddy-like features. These features dominate the variability in the 10-20 day band. They have not been described in previous studies. Their discovery was made possible by the use of high frequency radar which can observe evolving patterns of surface currents.

2. The propagating eddy-like patterns consist of two dominant components: (1) Mode 1, explaining 45% of the variance, is a pattern of westward-propagating counter-rotating vortices similar to the propagating cyclones reported by Harms and Winant (1998). (2) Mode 2, explaining 20% of the variance, is a pattern of alongshore fluctuations on the mainland coast similar to the coastal trapped waves described by Auad and Henderschott (1997). The pattern of fluctuating along-shelf currents described by mode 2 with a period of 13.3 days extends from the eastern entrance, through the radar coverage area, and beyond Pt. Conception indicating a long wavelength.

3. The propagating vortices described by mode 1 are consistent with the analytical model of topographic Rossby modes described by Pedlosky (1987). The observed stream function distribution (Fig. 13), propagation speed (4.7 km day-1) and period (14.3 days) are similar to those predicted by the model.

4. Frequency coupling between modes 1 and 2 suggests that the propagating vortices are a resonant interaction between the basin and the coastal trapped waves. The amplitude of mode 1 consistently increases when the frequency of mode 2 and the mean frequency of mode 1 converge. The amplitude of mode 1 consistently decreases as these frequencies diverge. The relationship only exists between the frequency of mode 2 and the mean frequency of mode 1, not the instantaneous frequency, suggesting that the interaction is regulated by shape of the Santa Barbara Basin.

These observations indicate that coastal trapped waves can interact with topographic features to produce strong secondary flows. In this case, the strong rotary flows are amplified in the basin and interact with the persistent cyclonic flow in the western Santa Barbara Channel. Similar interactions may occur more generally where basins are close enough to shore to be exposed to oscillatory flows from coastal trapped waves.

REFERENCES

Atkinson, L. P., K. H. Brink, R. E. Davis, B. H. Jones, T. Paluszkiewicz and D. W. Stuart (1986) "Mesoscale hydrographic variability in the vicinity of Points Conception and Arguello during April-May 1983: The OPUS 1983 experiment", Journal of Geophysical Research, 91, 12889-12918.

Auad, G., M. Henderschott and C. D. Winant (1998) "Wind-induced currents and bottom-trapped waves in the Santa Barbara Channel", Journal of Physical Oceanography, 28, 85-102.

Auad, G. and M. C. Henderschott (1997) "The low-frequency transport in the Santa Barbara Channel: description and forcing", Contintental Shelf Research, 17(7), 779-802.

Auad, G., M. C. Hendershott and C. D. Winant (1999) "Mass and heat balances in the Santa Barbara Channel: estimation, description and forcing [Review]", Progress in Oceanography, 43(1), 111-155.

Barth, J. A. and K. H. Brink (1987) "Shipboard acoustic doppler profiler velocity observations near Point Conception: Spring 1983", Journal of Geophysical Research, 92(C4), 3925-3943.

Battisti, D. S. and B. M. Hickey (1984) "Application of remote wind-forced coastal trapped wave theory to the Oregon and Washington Coasts", Journal of Physical Oceanography, 14, 887-903.

Beale, E. M. L. and R. J. A. Little (1975). Missing values in multivariate analsys. Computational practice in mathematical programming. New York, American Elsevier. vi**,** 168.

Beckenbach, E. H. (2004). "Surface circulation in the Santa Barbara Channel: An application of high frequency radar for descriptive physical oceanography of the coastal ocean". Ph.D. Dissertation, Interdepartmental Program in Marine Science. University of California, Santa Barbara**,** pp 126.

Beckenbach, E. H. and L. Washburn (2004) "Low frequency waves in the Santa Barbara Channel observed using high frequency radar", in press, Journal of Geophysical Research.

Brink, K. H. (1983) "The near-surface dynamics of coaastal upwelling", Progress in Oceanography, 12, 223-257.

Brink, K. H. (1991) "Coastal-trapped waves and wind driven currents over the continental shelf", Annual Review of Fluid Mechanics(23), 389-412.

Brink, K. H. and D. C. Chapman (1985). Programs for computing properties of coastal trapped waves and wind driven motions over the continental shelf and slope. Woods Hole, Woods Hole Oceanography Institute.

Brink, K. H. and R. D. Muench (1986) "Circulation in the Point Conception-Santa Barbara Channel region", Journal of Geophysical Research, 91, 877-895.

Chen, C.-S. and D. P. Wang (1999) "Data assimilation model study of the Santa Barbara Channel Circulation", Journal of Geophysical Research, 104, 15,727-15741.

Davis, R. E. and P. Bogden (1989) "Variability on the California Shelf forced by local and remote winds during the Coastal Ocean Dynamics Experiment", Journal of Geophysical Research, 94, 4763-4783.

Dever, E. P., M. C. Henderschott and C. D. Winant (1998) "Statistical Aspects of surface drifter observations of circulation in the Santa Barbara Channel", Journal of Geophysical Research, 103(C11), 24,781-24,797.

Emery, B. M., L. Washburn and J. Harlan (2004) "Evaluating CODAR high frequency radars for measuring surface currents: observations in the Santa Barbara Channel", Journal of Atmospheric and Oceanic Technology, submitted.

Gurgel, K. W. (1994) "Shipborne measurement of surface current fields by HF radar", L'Onde Electrique, 74(5), 54-59.

Harms, S. and C. D. Winant (1998) "Characteristic patterns of the circulation in the Santa Barbara Channel", Journal of Geophysical Research, 103(C2), 3041-3065.

Hendershott, M. C. and C. D. Winant (1996) "The circulation of the Santa Barbara Channel", Oceanography, 9(2), 114-121.

Hickey, B. M. (1992) "Circulation over the Santa Monica-San Pedro Basin and Shelf", Progress in Oceanography, 30, 37-115.

Huyer, A. (1983) "Coastal upwelling in the California current system", Progress in Oceanography, 12, 259-284.

Kolpack, R. J. (1971). Biological and Oceanographical Survey in the Santa Barbara Channel Oil Spill 1969-1970, vol 2. Los Angeles, University of Southern California**,** 447.

Miller, A. J., P. F. J. Lermusiaux and P.-M. Poulain (1996) "A topographic-Rossby mode resonance over the Iceland-Faroe Ridge", Journal of Physical Oceanography, 26, 2735-2747.

Nishimoto, M. M. and L. Washburn (2002) "Patterns of coastal eddy circulation and abundance of pelagic juvenile fish in the Santa Barbara Channel, California, USA", Marine Ecological Progress Series, 241, 183-199.

Oey, L.-Y. (1999) "A forcing mechanism for the poleward flow off the southern California coast", Geophysical Research, 101, 13,529-13,529.

Oey, L. Y., D. P. Wang, T. Hayward, C. Winant and M. Hendershott (2001) ""Upwelling" and "cyclonic" regimes of the near-surface circulation in the Santa Barbara Channel", Journal of Geophysical Research-Oceans, 106(C5), 9213-9222.

Orchard, T. and M. A. Woodbury (1972). A missing information principle: theory and applications. Proceedings of the 6th Berkekley Symposium on Mathematics, Statistics, and Probability.

Paduan, J. D. and L. K. Rosenfeld (1996) "Remotely sensed surface currents in Monterey Bay from shore-based HF radar (Coastal Ocean Dynamics Application Radar)", Journal of Geophysical Research, 101(C9), 20,669-20,686.

Pedlosky, J. (1987). Geophysical Fluid Dynamics. Ney York, Springer-Verlag.

Pedlosky, J. (1987). Geophysical Fluid Dynamics. New York, Springer-Verlag.

Pierini, S. (1996) "Topographic Rossby modes in the Strait of Sicily", Journal of Geophysical Research, 101(C3), 6429-6440.

Pierini, S. (1996) "Topographic Rossby modes in the Straite of Sicily", Journal of Geophysical Research, 101(C3), 6429-6440.

Sverdrup, H. V. (1938) "On the process of upwelling", Journal Marine Research, 2, 155-164.

Vastano, A. C. and R. O. Reid (1985) "Sea surface topography estimation with infrared satellite imagery", Journal of Atmospheric and Oceanic Technology, 2, 393-400.

Wallace, J. M. (1972) "Empirical orthogonal representation of time series in the frequency domain. Part I Theoretical considerations", Journal of Applied Meteorology, 11(6), 887-892.

Winant, C. D., D. J. Alden, E. P. Dever, K. A. Edwards and M. C. Henderschott (1999) "Near-surface trajectories off central and southern California", Journal of Geophysical Research, 104(C7), 15,713-15,726.

Winant, C. D., R. C. Beardsley and R. E. Davis (1987) "Moored wind, temperature, and current observations made during Coastal Ocean Dynamics Experiments 1 and 2 over the northern California continental shelf and upper slope", Journal of Geophysical Research, 92(C2), 1569-1604.

The Department of the Interior Mission

As the Nation's principal conservation agency, the Department of the Interior has responsibility for most of our nationally owned public lands and natural resources. This includes fostering sound use of our land and water resources; protecting our fish, wildlife, and biological diversity; preserving the environmental and cultural values of our national parks and historical places; and providing for the enjoyment of life through outdoor recreation. The Department assesses our energy and mineral resources and works to ensure that their development is in the best interests of all our people by encouraging stewardship and citizen participation in their care. The Department also has a major responsibility for American Indian reservation communities and for people who live in island territories under U.S. administration.

The Minerals Management Service Mission

As a bureau of the Department of the Interior, the Minerals Management Service's (MMS) primary responsibilities are to manage the mineral resources located on the Nation's Outer Continental Shelf (OCS), collect revenue from the Federal OCS and onshore Federal and Indian lands, and distribute those revenues.

Moreover, in working to meet its responsibilities, the **Offshore Minerals Management Program** administers the OCS competitive leasing program and oversees the safe and environmentally sound exploration and production of our Nation's offshore natural gas, oil and other mineral resources. The MMS **Royalty Management Program** meets its responsibilities by ensuring the efficient, timely and accurate collection and disbursement of revenue from mineral leasing and production due to Indian tribes and allottees, States and the U.S. Treasury.

The MMS strives to fulfill its responsibilities through the general guiding principles of: (1) being responsive to the public's concerns and interests by maintaining a dialogue with all potentially affected parties and (2) carrying out its programs with an emphasis on working to enhance the quality of life for all Americans by lending MMS assistance and expertise to economic development and environmental protection.